JOURNAL OF SOLID STATE CHEMISTRY 14, 395–406 (1975)

Perovskite-like $La_{1-x}K_xMnO_3$ and Related Compounds: Solid State Chemistry and the Catalysis of the Reduction of NO by CO and H_2

R. J. H. VOORHOEVE, J. P. REMEIKA, L. E. TRIMBLE, A. S. COOPER, F. J. DISALVO, AND P. K. GALLAGHER

Bell Laboratories, Murray Hill, New Jersey 07974

Received December 3, 1974

The new compounds $La_{1-x}M_xMnO_3$ ($0.05 \leqslant x \leqslant 0.4$ for $M = K$; $x = 0.2$ for $M = Na$, Rb) have been prepared. $La_{1-x}K_xMnO_3$ ($0.05 \leqslant x \leqslant 0.4$), $LaMnO_{3.01}$, $LaMnO_{3.15}$, $La_{0.8}Na_{0.2}MnO_3$, and $La_{0.8}Rb_{0.2}MnO_3$ have been used as catalysts in the reduction of NO. $La_{0.8}K_{0.2}MnO_3$ has also been used in the catalytic decomposition of NO. The activity of these catalysts is related to the presence of a Mn^{3+}/Mn^{4+} mixed valence and to the relative ease of forming oxygen vacancies in the solid. The presence of cation vacancies in $LaMnO_{3.15}$ and the substitution of La^{3+} by alkali ions in $LaMnO_3$ increases the catalytic activity. The reduction of NO involves both molecular and dissociative adsorption of NO.

Introduction

Perovskite-like compounds derived from $LaMnO_3$ by partial substitution of La^{3+} by divalent ions have long been known (*1*, *2*). Their electrical and magnetic properties have been extensively studied and related to the crystal structure and defect chemistry (*3–7*). These and related systems appear to offer an opportunity to relate catalytic properties to solid state chemistry. This is in particular so, since these compounds contain a catalytically active Mn ion in oxygen octahedra linked by inactive La ions in dodecahedral coordination. Also, substitution of La by other catalytically inactive ions makes it possible to vary the electronic configuration of the MnO_6 units while maintaining the same or very nearly the same geometry of the active center.

The purpose of the present paper is to study the compounds in which La is substituted by alkali ions in comparision with $LaMnO_3$. The general formula is $La_{1-x-y}\square_y M_xMnO_3$, in which $\square$ is a cation vacancy on the dodecahedral La-site (*A*-site) and *M* is Na, K, or Rb. Since La^{3+} is replaced by M^+ and/or by formally neutral $\square$, the above formula demands charge compensation to the effect that a fraction of $(3y + 2x)$ of the Mn is tetravalent with the remainder of the Mn trivalent. The members $LaMnO_3$ and $La_{1-y}\square_yMnO_3$ ($y \lesssim 0.13$) were already known (*3*, *8*), but the preparation of alkali-substituted $LaMnO_3$ ($0 < x \leqslant 0.4$) is reported here for the first time. The crystal structure, the electrical conductivity, and the activity and selectivity in the catalytic reduction of NO are reported for powder samples.

Substituted manganites are indeed active catalysts. $La_{0.65}Sr_{0.35}MnO_3$ has been used in CO oxidation (*9*), $La_{0.7}Pb_{0.3}MnO_3$ has been used in CO oxidation and NO reduction (*10*, *11*), and $La_{1-x}Ca_xMnO_3$ has been used in NH_3 oxidation (*12*). The electrical and magnetic properties of these manganites are dominated by the negative superexchange interaction Mn^{3+}–O–Mn^{3+} and the strong positive Mn^{3+}–O–Mn^{4+} interaction due to double exchange (*3*, *7*). In first approximation, these interactions are independent of the nature of the *A*-site substitution ($\square$ or M^+) and depend mainly on the Mn^{4+}/Mn^{3+} ratio (*3*). On the other hand, the binding energy for an oxygen atom in the lattice

TABLE I

CHARACTERIZATION OF $La_{1-x}M_xMnO_3$ CATALYSTS

Number	Formula	Catalyst[a]	Firing °C Hours	X ray[b]	Mn^{4+}/Mn (%) Calculated[c]	Mn^{4+}/Mn (%) Analyzed[d]	Vacancies on *A*-site (%)	Surface area (m^2/g)
1	$LaMnO_3$	*F*	1200 N_2 16	*O*	—	2	0.7	0.40
		S		*O*	—	2	0.7	0.45
2	$LaMnO_3$	*F*	900 O_2 16	*R*	—	30	10	0.40
		S		*O*	—	9	3	1.00
3	$La_{0.8}Na_{0.2}MnO_3$	*F*	1100 air 16	*R*	40			0.90
		S		*R*[f]				0.88
4	$La_{0.8}Rb_{0.2}MnO_3$	*F*	1100 air 16	*R*[e]	40			0.88
		S		*R*[f]				
5	$La_{0.95}K_{0.05}MnO_3$	*F*	1100 air 16	*O*	10			0.62
		S		*O*				1.20
6	$La_{0.9}K_{0.1}MnO_3$	*F*	1000 air 16	*R*	20			1.8
		S		*R*				2.0
7	$La_{0.8}K_{0.2}MnO_3$	*F*	1000 air 16	*R*[e]	40			2.5
		S		*R*[f]				2.5
8	$La_{0.7}K_{0.3}MnO_3$	*F*	1100 air 16	*R*[e]	60			0.92
		S		*R*[f]				1.1
9	$La_{0.6}K_{0.4}MnO_3$	*F*	1100 air 16	*R*[e]	80			0.85
		S		*R*[f]				1.80

[a] *F* for compound before use as catalyst, *S* for spent catalyst.
[b] *O* for orthorhombic distortion of cubic symmetry, *R* for rhombohedral distortion.
[c] Calculated on the basis of the formula.
[d] Analyzed for Mn^{4+} and total Mn, or in case of $LaMnO_3$, calculated from Table II and literature data.
[e] A small impurity, probably a K_2O–Mn_2O_3 compound, was found in the fresh catalyst.
[f] In these spent catalysts weak or very weak lines of MnO were observed by X ray.

depends very much on whether it is next to La^{3+}, M^+, or □.

The test reactions employed for the catalytic measurements are

$$2NO + 2CO \rightarrow N_2 + 2CO_2 \quad (1)$$

$$2NO + 2H_2 \rightarrow N_2 + 2H_2O \quad (2)$$

In both reactions, N_2O can be formed in addition to N_2. Moreover, formation of NH_3 can occur:

$$2NO + 5H_2 \rightarrow 2NH_3 + 2H_2O \quad (3)$$

The activity of the manganites in the catalytic conversion of NO and the selectivity of the reaction towards N_2, N_2O, and NH_3 will be used to characterize their catalytic properties. These catalytic properties are of importance in the treatment of exhaust gases of internal combustion engines (*11*). In such applications, catalysts must be selective toward formation of N_2 and N_2O rather than NH_3.

Experimental

The manganites were used as loose powders. They were prepared by firing mixtures of the oxides or carbonates in the appropriate proportions in air or oxygen at 800–1400°C, with frequent regrinding and refiring of the products. Subsequent firing in O_2 was used to prepare samples with high Mn^{4+} content, while firing in N_2 was used for low Mn^{4+} contents (Table I).

The stoichiometry of the samples was determined by analyzing for Mn^{3+}, Mn^{4+} La^{3+}, and M^+.

The electrical conductivities were determined on sintered pressed pellets of the compounds. Square bars 15 mm long with 3-mm cross sections were sawed from the pellets and a four-point method with spring-loaded Pt contacts was used.

The crystal structures were determined from powder X ray diffraction patterns taken in a Philips 114.6-mm diameter Debye–Scherrer camera using Cr$K\alpha$ radiation. The measured lattice parameters of each starting material are listed in Table II.

The surface areas of the catalysts were measured by the BET method (*13*), using N_2 adsorption in a Shell–Perkin Elmer Sorption Meter. The catalytic properties were determined on 0.3 cm^3 of the compound placed in a fixed-bed continuous flow reactor (*14*). The compositions of the inlet gases and reactor effluents were measured by gas chromatography of gas samples taken at 10-min intervals. Directly determined were NO, CO, H_2, N_2O, and N_2, while NH_3 was determined from the nitrogen mass balance (*15*). The NH_3 analysis was occasionally confirmed by mass spectrometric analysis. The results

TABLE II

LATTICE PARAMETERS OF $La_{1-x}M_xMnO_3$

Number	Formula	Symmetry[a]	V^b (Å^3)	a (Å)	b (Å)	c (Å)
1*F*	$LaMnO_{3.01}$	*O*	61.00	5.536 (1)	5.726 (1)	7.697 (2)
2*F*	$LaMnO_{3.15}$	*R*	58.66	5.523 (1)		13.324 (2)
3*F*	$La_{0.8}Na_{0.2}MnO_3$	*R*	58.27	5.506 (3)		13.317 (8)
4*F*	$La_{0.8}Rb_{0.2}MnO_3$	*R*	59.45	5.541 (2)		13.415 (5)
5*F*	$La_{0.95}K_{0.05}MnO_3$	*O*	59.45	5.538 (5)	5.521 (5)	7.789 (6)
6*F*	$La_{0.9}K_{0.1}MnO_3$	*R*	58.90	5.524 (1)		13.374 (3)
7*F*	$La_{0.8}K_{0.2}MnO_3$	*R*	58.83	5.519 (1)		13.381 (2)
8*F*	$La_{0.7}K_{0.3}MnO_3$	*R*	58.63	5.511 (2)		13.376 (6)
9*F*	$La_{0.6}K_{0.4}MnO_3$	*R*	58.65	5.511 (1)		13.380 (2)

[a] *O* for orthorhombic, *R* for rhombohedral.
[b] Volume per ABO_3 unit.

for NO, N_2O, N_2, and NH_3 are presented as a percentage of NO inlet remaining or converted into N-containing products. The gases used included a dry mixture (*D*) of 0.13% NO, 0.4% H_2, and 1.3% CO in He and a wet mixture (*W*) of 0.13% NO, 0.4% H_2, 1.3% CO, 3% H_2O, and 3% CO_2 in He. Other mixtures were as indicated in the text. Flow rates are expressed as *RSV* (ml gas NTP/hr/m^2 of catalyst surface area in the reactor based on the surface area of the fresh catalyst).

The catalysts used, with details on preparation and characterization, are listed in Table I. Unless noted otherwise, the catalytic behavior shown is the stable behavior, after any initial transients have passed.

Results

Structural, Electrical, and Magnetic Properties

$LaMnO_3$ was prepared in a nearly stoichiometric orthorhombic state and in an oxygen-rich rhombohedral state by firing in either neutral or oxidizing conditions (Table I, catalysts No. 1 and No. 2, respectively). From the lattice parameters (Table II) the oxygen content was deduced with the aid of a compilation of the available structural data (*6*, *8*, *12*, *16–20*). $LaMnO_3(O)$ contained 2% Mn^{4+}, whereas $LaMnO_3(R)$ contained 30% Mn^{4+}. The Mn^{4+} content is compensated by the presence of cation vacancies. No La_2O_3 was observed to exsolve, putting its concentration at lower than 2%. A structure with predominantly La vacancies, in addition to a small number of Mn vacancies, is in accord with these observations. On the basis of neutron diffraction refinement, a structure $La_{0.95\pm0.02}Mn_{0.96\pm0.04}O_3$ with 9% of the cation sites vacant in a complete oxygen sublattice was recently proposed for rhombohedral $LaMnO_{3.12}$ (*8*).

Alkali-substituted manganites were prepared with the nominal formulas $La_{1-x}K_xMnO_3$ ($x = 0.05$, 0.1, 0.2, 0.3, and 0.4), $La_{0.8}Na_{0.2}MnO_3$ and $La_{0.8}Rb_{0.2}MnO_3$. In view of the sizes of Mn^{3+} (0.66 Å), La^{3+} (1.22 Å), and the alkali ions (Na^+ 0.97 Å, K^+ 1.38 Å, Rb^+ 1.56 Å), it is expected that the latter will enter the dodecahedral La-site and not the octahedral Mn-site. Indeed, attempts to prepare $LaNa_{0.2}Mn_{0.8}O_3$ with Na^+ in the octahedral site were unsuccessful since they did not lead to single-phase samples. All samples mentioned above except $La_{0.95}K_{0.05}MnO_3$ were perovskites with rhombohedral distortions of the cubic symmetry similar to those in $LaMnO_3$ (*R*) There was no evidence of ordering of the *M* ions. The lattice parameters (Table II) are expected to be dependent on the actual Mn^{4+} content which, due to the presence of *A*-site vacancies, may be higher than calculated from the alkali-ion content. For the lower alkali contents ($x \leqslant 0.2$), nonstoichiometry of the compounds is likely to be restricted to the presence of cation vacancies, with the oxygen sites being very nearly filled, similar to the situation in $LaMnO_{3.12}$ (*8*). For higher values of x ($x > 0.2$) the presence of oxygen vacancies and a related reduction of the Mn^{4+}/Mn^{3+} ratio below the nominal value of $2x/(1-2x)$ is expected in analogy with the data for $La_{1-x}Sr_xMnO_3$, $La_{1-x}Ca_xMnO_3$, and $La_{1-x}Sr_xCoO_3$ for $x \geqslant 0.4$ (*1*, *12*, *21*, *22*).

Electrical conductivity measurements showed $La_{0.9}K_{0.1}MnO_3$ and $La_{0.8}K_{0.2}MnO_3$ to be semiconductors with activation energies for electrical conduction of 0.14 ± 0.01 and 0.075 ± 0.005 eV, respectively. At 400°C, a temperature in the range where catalytic activity is measured, the resistivity is approximately 0.005 Ωcm for both samples. Similar resistivity is expected for $LaMnO_3(R)$ with 30% Mn^{4+}, a value intermediate between those for $La_{0.9}K_{0.1}MnO_3$ and $La_{0.8}K_{0.2}MnO_3$. On the other hand, stoichiometric $LaMnO_3$ (*O*) reportedly has a semiconducting activation energy of 0.36 eV and resistivity at 400°C of 1 Ωcm (*23*). The electrical conductivities are the result of the charge hopping between Mn^{3+} and Mn^{4+} ions, analogous to that occurring in $La_{1-x}Sr_xMnO_3$ (*3*) (which also has a similar resistivity at 400°C).

Catalytic Activity of $LaMnO_3(O)$ and $LaMnO_3(R)$

Many oxide catalysts function in oxidation–reduction reactions by participation of their lattice oxygen in the reaction (*24*, *25*). This has been substantiated for $La_{0.8}K_{0.2}MnO_3$ (see below). Since in the manganites, oxidation

and reduction of the catalysts occur through adjustments of the concentrations of *A*-site vacancies, the bulk oxidation and reduction are expected to occur only slowly at reaction temperatures ($T < 600°C$), their rates are limited by solid state diffusion. This was indeed found to be true for $LaMnO_3$ to a degree sufficient for making meaningful catalytic measurements.

In Fig. 1, catalytic measurements are summarized for $LaMnO_{3.01}$ (No. 1, Table 1, orthorhombic) and $LaMnO_{3.15}$ (No. 2, rhombohedral). The top panel gives the percentage of inlet NO remaining in the effluent from the reactor; the middle and lower panels give the percentage of inlet NO converted into NH_3 and N_2, respectively. Solid curves are for the NO–CO–H_2–He mixture, dashed lines are for the H_2O–NO–CO–CO_2–H_2–He mixture. The stability of the two catalysts is not very great, as is indicated by the slowly varying results for the consecutive runs *A*–*D* for $LaMnO_{3.15}$ and in run *H* for $LaMnO_{3.01}$.

NO conversion on $LaMnO_{3.15}$ is much faster than on $LaMnO_{3.01}$, since the temperatures necessary for 50% NO conversion are $T_{50} = 380°C$ and $T_{50} = 530°C$, respectively. The difference is mainly due to the rate of N_2 production, while the rate of NH_3 formation is about the same on both catalysts. The two compounds also behave in a quite different manner when H_2O is added to the gas stream: $LaMnO_{3.15}$ is hardly affected, while on $LaMnO_{3.01}$ the rate of N_2 production drops to

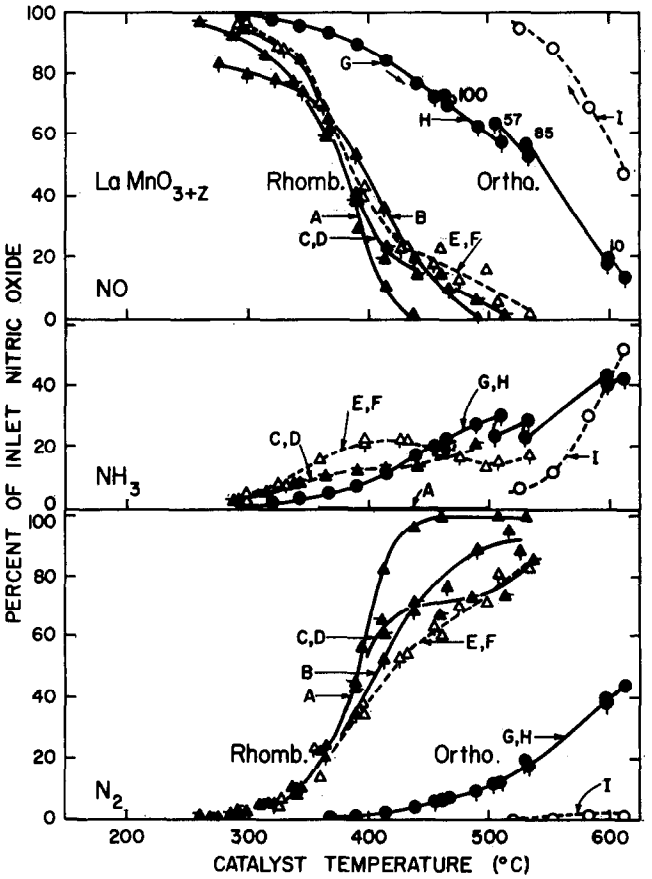

FIG. 1. Composition of reactor effluent for $LaMnO_3(O)$ and $LaMnO_3(R)$ catalysts. Flowrate (*RSV*) 23 500 ml hr^{-1} m^{-2} based on surface area of fresh catalyst (Table 1). Full lines and filled-in symbols: gas mixture *D*. Dashed lines and open symbols: gas mixture *W*. N_2O yield unimportant except in runs *A* and *B*.

almost zero and the total NO conversion shifts to a much lower level (curves *G*, *H*, and *I* in Fig. 1).

The difference in behavior of $LaMnO_{3.15}$ and $LaMnO_{3.01}$ cannot be due to the difference in structure (rhombohedral versus orthorhombic distortion). This is shown by the fact that $LaMnO_{3.15}$ during testing (runs *A–F*) changed from the rhombohedral to the orthorhombic structure, while being reduced to $LaMnO_{3.05}$. The change is accompanied by some loss of activity (compare *A* to *B*, *C*, and *D*), but the orthorhombic $LaMnO_{3.05}$ is clearly still appreciably more active than the orthorhombic $LaMnO_{3.01}$. Hence, the different activities of $LaMnO_{3.15}$ and $LaMnO_{3.01}$ must be due to the different oxidation states.

Note that the product zA of the excess oxygen z in the formula $LaMnO_{3+z}$ and surface area A is 0.056 for No. 2*F*, 0.050 for No. 2*S*, and 0.004 for Nos. 1*F* and 1*S*. This may be regarded as a measure of the number of active sites available for the catalysis and shows the compensation of decreasing z and increasing surface area for catalyst No. 2. Note also that on fresh $LaMnO_{3.15}$, no NH_3 is produced at all.

Catalytic Activity of $La_{0.8}M_{0.2}MnO_3$ (M = Na, K, Rb)

As shown above, $LaMnO_{3.15}$ is of fairly low stability in the reducing atmosphere of the test reaction. However, similar Mn^{4+} concentrations can be maintained stably in charge-compensated $La_{0.08}M_{0.2}MnO_3$, where the charge compensation is by an alkali ion rather than by a La vacancy. Fig 2. shows that $La_{0.8}Na_{0.2}MnO_3$ (No. 3, Table I) and $La_{0.8}Rb_{0.2}MnO_3$ (No. 4) are indeed active catalysts, appreciably more so than $LaMnO_{3.01}$ (No. 1). Similar to $LaMnO_{3.15}$ (No. 2), NO is mainly converted to N_2 and N_2O rather than to NH_3. The curves for $La_{0.8}K_{0.2}MnO_3$ are similar to those shown in Fig. 2. The effect of adding water to the gas mixture on the latter catalyst was the same as observed for $LaMnO_{3.15}$.

Since the sodium and rubidium compounds, which are both rhombohedral, have quite different lattice constants (Table II), due to the much higher radius of Rb^+ in comparison with Na^+, their similar activity indicates that the size of the alkali ions and the distortion of the rare earth polyhedra are not important for the catalytic activity.

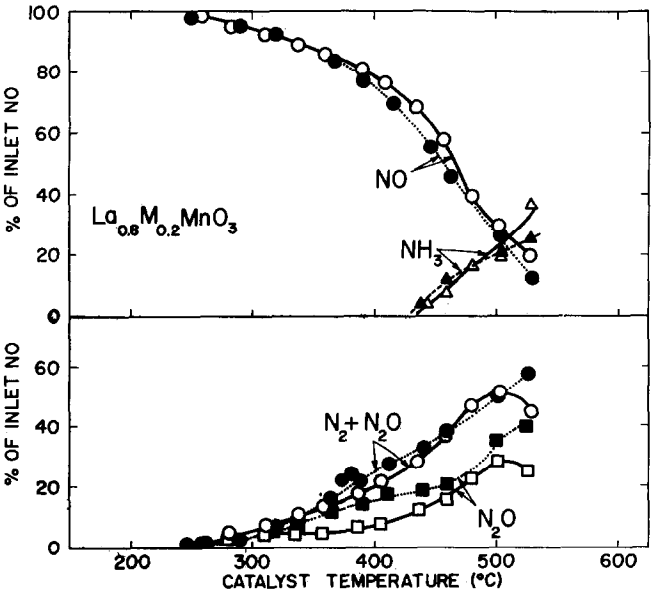

FIG. 2. Composition of reactor effluent for $La_{0.8}Na_{0.2}MnO_3$ (RSV = 13 100 ml h^{-1} m^{-2}, full lines, open symbols) and for $La_{0.8}Rb_{0.2}MnO_3$ (RSV = 14 300 ml hr^{-1} m^{-2}, dashed lines, filled symbols). Mixture *D*.

$La_{0.8}M_{0.2}MnO_3$ and $LaMnO_{3.15}$ show similar selectivities (proportions of NH_3 in the product). However, note that the activity of $La_{0.8}M_{0.2}MnO_3$ is appreciably lower with $T_{50} = 450°C$, while for $LaMnO_{3.15}$, $T_{50} = 380°C$. This is remarkable since the Mn^{4+} concentrations are somewhat higher. Also, the yield of N_2O is higher relative to that of N_2, indicating that N_2O reduction and decomposition are slower than on $LaMnO_{3.15}$.

Catalytic activity of $La_{1-x}K_xMnO_3$ ($0 \leqslant x \leqslant 0.4$)

The variation of the catalytic activity of the potassium compounds $La_{1-x}K_xMnO_3$ with the value of x is given by the data in Fig. 3. The curves for $x = 0.1$ should be shifted slightly to lower temperatures to correct for a specific flow rate (volume of gas treated per m^2 of surface area of catalyst per hour) which was twice that of the other tests. The top panel of Fig. 3 shows that the activity rises gradually with increasing values of x, i.e., T_{50} decreases from a (corrected) value of 480°C for $x = 0.1$ to 400°C for $x = 0.3$. The further rise in NO conversion rate from $x = 0.3$ to $x = 0.4$ is completely due to the production of more NH_3 rather than to an increased production rate of N_2 and N_2O. This may well be related to the fact that the Mn^{4+} concentration in similar systems, e.g., $La_{1-x}Sr_{1-x}MnO_3$ (*1*) and $La_{1-x}Ca_xMnO_3$ (*12*) rises only slowly once a level of 40–50 % Mn^{4+} has been reached. Further introduction of the compensating element then leads to the formation of oxygen vacancies.

The low activity of $La_{0.95}K_{0.05}MnO_3$ should be compared with that of $LaMnO_{3.01}$ in Fig. 1. The latter, which has 2 % Mn^{4+}, is more active than the former, with 10 % Mn^{4+}, but the selectivity towards N_2 and NH_3 is similar. It is likely that the different activities are related to the concentration of *A*-site vacancies in $La_{0.95}K_{0.05}MnO_3$; K^+ is expected to fill these vacancies.

Mechanism of the NO Reduction Process over $La_{0.8}K_{0.2}MnO_3$

(*a*) *Lattice oxygen and O_2 in the gas phase.* To establish whether lattice oxygen plays a

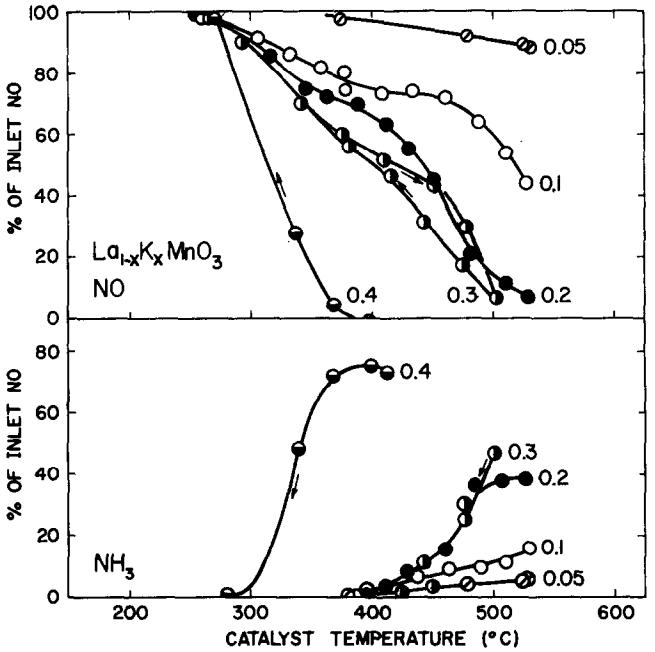

FIG. 3. Composition of reactor effluent for $La_{1-x}K_xMnO_3$. *RSV* for $x = 0.05$ was 19 000 ml m^{-2} hr^{-1}; for $x = 0.1$, 27 200; for $x = 0.2$, 13 200; for $x = 0.3$, 12 000; and for $x = 0.4$, 13 800. Data for N_2 and N_2O omitted for clarity. Arrows indicate ascending or descending temperature. Mixture *D*.

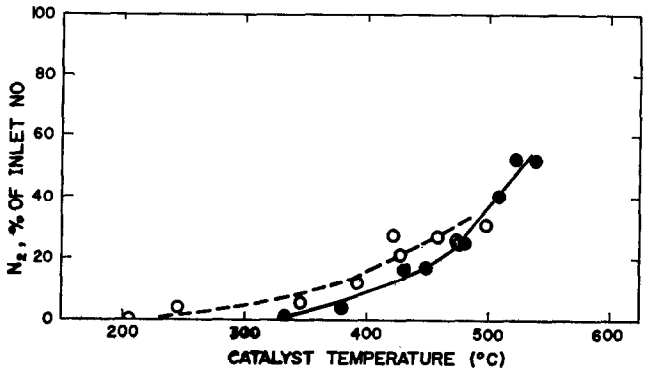

FIG. 4. Yield of N_2 in catalytic decomposition of NO on prereduced $La_{0.8}K_{0.2}MnO_3$ (solid line) and in catalytic reduction with mixture *D* (dashed curve). $RSV = 5000$ ml m^{-2} hr^{-1}.

role in the NO reduction, or in other words, whether the reaction proceeds through a consecutive reduction of the catalyst by CO or H_2 followed by reoxidation of the catalyst by NO, the latter was reacted over the $La_{0.8}K_{0.2}MnO_3$ catalyst both in the presence and in the absence of reducing gases. In the experiment, a mixture of 0.13% NO, 0.4% H_2 and 1.3% CO in He was first passed over the catalyst at a rate of 5000 ml/m^2 surface area/hr. In Fig. 4, the dashed curve shows the production of $N_2O + N_2$. Subsequently, when the reducing gases were omitted and 0.13% NO in He was passed over the catalyst, a similar reaction rate of NO to N_2O was observed (full curve in Fig. 4). The oxygen removed from the NO molecules is retained by the catalyst, which takes up more than the equivalent of 10 monolayers of O_2 before the NO conversion slows down. This indicates that the process occurring is

$$V_o + 2e + NO \rightarrow N_{ads} + O^{2-}\text{(lattice)} \quad (4)$$

$$2N_{ads} \rightarrow N_2 \quad (5)$$

$$N_{ads} + NO_{ads} \rightarrow N_2O \quad (6)$$

This process is in accordance with the observation (*26, 27*) that the catalytic decomposition of NO is inhibited by oxygen in the gas phase, which decreases the number of lattice oxygen vacancies V_o.

The addition of O_2 to a gas flow consisting of 0.13% NO, 1.3% CO, 3% CO_2, and 3% H_2O in He, in amounts less than the stoichiometric amount of 0.65%, decreases the conversion of NO to N_2O and N_2 (Fig. 5). O_2 reacts in preference to NO. This shows preferential adsorption of O_2 on NO adsorption sites, as was found before for other oxide catalysts (*27*). It is mainly the N_2O production that is affected and not the rate of N_2 production. For example, at 490°C in the absence of O_2, NO is converted for 21% into N_2 and for 16% into N_2O. With 0.13% O_2 present, these numbers are 24% and 4%, respectively. Therefore, it is likely that O_2 interferes more strongly with the molecular NO adsorption [in Eq. (6)], than with the dissociative NO adsorption [in Eqs. (4) and (5)].

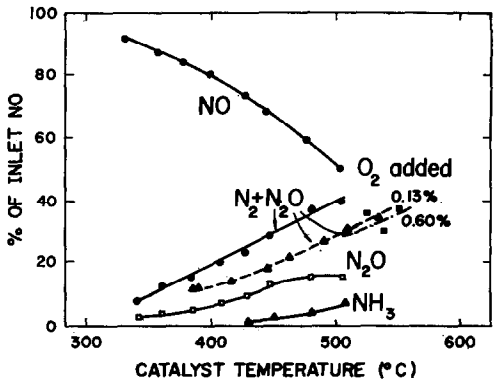

FIG. 5. Composition of reactor effluent for $La_{0.8}K_{0.2}MnO_3$ for a feed mixture of 0.13% NO, 1.3% CO, 3% H_2O, and 3% CO_2 in He, with O_2 added in amounts of 0%, 0.13%, and 0.6%. Full curves: composition for 0% O_2. Dashed lines: conversion of NO to $N_2 + N_2O$ when O_2 is added. $RSV = 13\,200$ ml m^{-2} hr^{-1}.

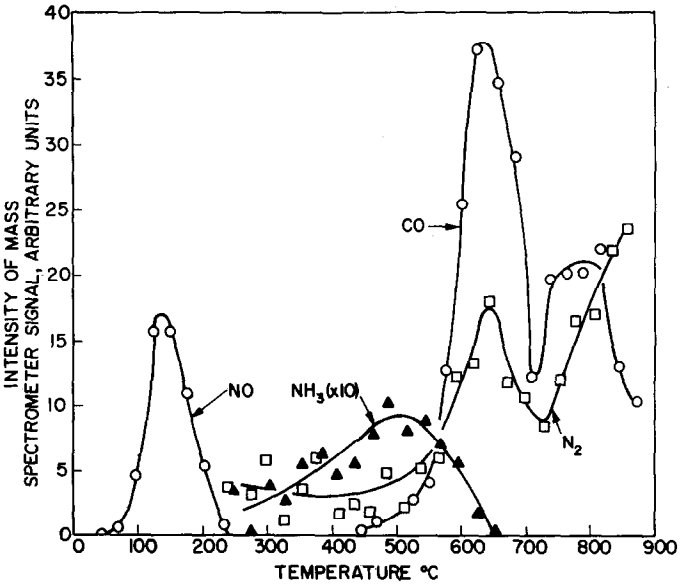

FIG. 6. Mass spectrometric desorbed gas analysis of $La_{0.8}K_{0.2}MnO_3$ treated in mixture *D* and in 1% NO in He (see text). Heating rate 2°C/min. N_2 data from $m/e = 14$, NH_3 data from $m/e = 17$ corrected for the contribution of OH to that mass peak, CO data from $m/e = 28$ corrected for the contributions of N_2 and CO_2, NO data from $m/e = 30$. CO_2 shows a peak at 630°C (not shown).

(*b*) *Molecular and dissociative adsorption of NO.* To establish the relative importance of molecular and dissociative adsorption of NO on these manganites, a sample of $La_{0.8}K_{0.2}MnO_3$ was used in the conversion of a mixture of 0.13% NO, 0.4% H_2, and 1.3% CO in He at 620°C for 1 hr, cooled in this mixture to 150°C and held at 150°C in 1% NO in He, after which it was cooled to room temperature. The sample was transferred under 1% NO in He to a fused silica thermal desorption apparatus in which it was evacuated and its temperature was increased at 2°C/min. The desorbed gas was analyzed by mass spectrometry. Some of the major desorbing species are shown in Fig. 6. A control experiment in which NO was omitted showed none of the desorbed species in Fig. 6, except a small amount of CO desorbing at $T > 600$°C.

The results in Fig. 6 indicate that NO is moderately strongly chemisorbed in a molecular form, desorbing at 100–250°C. Assuming first-order desorption kinetics with a 10^{13} sec^{-1} frequency factor, a binding energy of 28 kcal/mol (1.2 eV) was derived. The appearance of NH_3 at $T > 300$°C and of N_2 at $T > 450$°C establish the presence on the surface of tightly bound N-containing radicals, which may be N_{ads}, NH_{ads}, etc. The simultaneous desorption of CO and N_2 at $T \approx 630$°C suggests the presence of a surface compound decomposing at that temperature. Since the ratio of N:CO ≈ 1, this might be an isocyanate compound. A high concentration of molecularly adsorbed NO appears to correlate with an enhanced NO conversion at 200–300°C observed on many manganite catalysts (*28*) and this conversion leads to significant amounts of N_2O, supporting the plausibility of Eq. (6).

(*c*) *Reduction of NO with CO–H_2 or CO–H_2O.* To gain some insight into the overall processes in the NO reduction, various gas mixtures were used. In Figs. 2 and 3, the product pattern for reduction of NO with a CO/H_2 mixture was presented, while in Fig. 5, a mixture of CO, H_2O, and CO_2 is the reducing agent. In this atmosphere, H_2 can only be formed by the water–gas shift reaction

$$CO + H_2O \rightleftarrows CO_2 + H_2 \qquad (7)$$

TABLE III

NO CONVERSION OVER $La_{0.8}K_{0.2}MnO_3$ AT 507°C, $RSV = 13\,200\ cm^3\ m^{-2}\ hr^{-1}$

Product, % of NO inlet	NO–CO–H_2[a]	NO–CO–H_2O[b]	NO–CO–CO_2	NO–CO–H_2O–CO_2[c]
N_2	20	24.5	19	22.5
N_2O	31	16	6.5	15.5
NH_3	38	32	0	6
$N_2 + N_2O$	51	40.5	25.5	38
Total	89	72.5	25.5	44

[a] Percentage of gas components, in the same order as given, in He: mixture 1, 0.13–1.3–0.4; mixture 2, 0.13–1.3–3.0; mixture 3, 0.13–1.3–3.0; mixture 4, 0.13–1.3–3.0–3.0.
[b] The water–gas shift proceeds and H_2 is found in the exit gas.
[c] The water–gas shift does not proceed.

Since the data for Na, K, and Rb are very similar we can compare Figs. 2 and 5. The NO conversion is very similar up to 430°C, when in the presence of H_2 the formation of NH_3 starts to increase steeply. Since in the presence of CO_2, no H_2 was found in the exit gas of the reactor, implying that Eq. (7) did not proceed, the similarity of the N_2 and N_2O production rates in Figs. 2 and 5 indicates that CO is the main reducing agent at $T < 430$°C.

At 507°C, the relative contributions of CO and H_2 to the NO reduction were further explored (Table III). In the second column the reducing mixture is CO + H_2. In the third column the shift reaction was observed by the occurrence of H_2 in the reactor effluent, while in the fifth column this was not the case. The yield of N_2 in these tests was remarkably constant at 21 ± 2% of the NO inlet, irrespective of the gases admixed to the NO–CO mixture. On the other hand, NH_3 is mainly produced by H_2, either provided as such or through the shift reaction (compare the second and third colums). At this fairly high temperature, N_2O formation is promoted by molecular H_2 (cf. the second and fourth columns) and to a lesser extent by the presence of H_2O, irrespective of the net rate with which the watergas shift proceeds (the third and fifth columns). OH groups at the surface might enhance the molecular adsorption of NO, providing an explanation for the enhanced N_2O formation through Eq. (6).

Discussion and Conclusions

In the present study, the conversion of NO over an isostructural series of manganites has been studied. The active site in all of these is very likely to be the same Mn ion or Mn–O–Mn group. In the perovskite structures, the (100) face containing a Mn–O–Mn square array is likely to be the most stable face (*29*, *30*). None of the modifying ions used, such as La^{3+}, Na^+, K^+, and Rb^+, has any appreciable catalytic activity for the reaction studied.

The oxygen of the perovskite lattice plays an important role in the NO conversion process, as indicated by the possibility of converting NO to N_2 and N_2O with a reduced oxide. The importance of lattice oxygen is also most strikingly demonstrated by the comparison of $LaMnO_{3.01}$ and $LaMnO_{3.15}$, the latter being a much more active catalyst than the former. In the catalytic decomposition (as opposed to reduction) of NO, the release of oxygen from the catalyst is the slow step in the reaction sequence. In the reduction of NO by CO, the binding of oxygen in the lattice also has an important role in the kinetics of the reaction. For example, when comparing $LaMnO_{3.15}$ (30% Mn^{4+}) with $La_{0.9}K_{0.1}MnO_3$ and $La_{0.8}K_{0.2}MnO_3$ (20 and 40% Mn^{4+}, respectively), it is readily apparent that for catalysts with comparable Mn^{4+} content, it is the nature of the charge-compensating defect that determines the catalytic activity.

When this is a cation vacancy, the activity is higher than when it is an alkali ion. Similarly, it was found (*31*) that the activity is higher for $La_{0.8}K_{0.2}MnO_3$ than for $La_{0.6}Sr_{0.4}MnO_3$ (both have 40% Mn^{4+}). These comparisons point to the binding energy of oxygen in the lattice, which decreases in the order (La, Sr) MnO_3 > (La, K) MnO_3 > (La, □) MnO_3. Lower binding energies for oxygen are thus correlated with higher catalytic activity for NO reduction. Note that in a different test reaction (the oxidation of NH_3) the vacancy concentration did not seem to be important, with (La, □) MnO_3 and (La, Ca)MnO_3 equally active at similar Mn^{4+} content (*12*). The release of oxygen from the lattice is probably not involved in the slow steps of that test reaction.

The introduction of cation vacancies lowers the binding energy for oxygen in the Mn–O–Mn structure, but also increases the Mn^{4+} content and the electrical conductivity. By comparisons of catalysts at constant Mn^{4+} content, it was possible to isolate the role of the binding of oxygen. The role played by Mn^{4+} and by the electrical conductivity is more difficult to isolate. However, in several of the reaction steps electronic charge transfer is occurring, e.g., in

$$NO + V_o + 2e \rightarrow N_{ads} + O^{2-}(\text{lattice}) \quad (8)$$

and in

$$O^{2-} + CO_{ads} \rightarrow CO_2 + V_o + 2e \quad (9)$$

In the first step, the presence of Mn^{3+} next to the oxygen vacancy V_o will facilitate the reaction, while in the second step the presence of Mn^{4+} next to O^{2-} will enhance the process, in both cases because the manganese ion can change valence while accepting or donating an electron. The electrical conductivity makes transfer of several electrons to and through one active center possible without grossly upsetting the local equilibrium valence situation. Low electrical conductivity is most likely to limit the charge transfer processes at the surface at compositions close to stoichiometric $LaMnO_3$. Studies of that range are presently underway.

The dissociative adsorption of NO [Eq. (8)] needs the presence of oxygen vacancies adjacent to an electron donor such as Mn^{3+}. The mere existence of oxygen vacancies in a structure, as in $Pb_2Ru_2O_{7-x}$, where they are fully coordinated by four Pb^{2+} ions, is not sufficient to enhance the activity (*28*). Sufficiently strong binding of oxygen in the vacancy to a transition metal ion is evidently necessary. On the other hand, molecular adsorption of NO is more likely to occur as a nitrosyl complex (*32*), competing with CO which is bound as the carbonyl. Such bonding is stronger on metal ions of low valence (*33*). The combined dissociative and molecular adsorption of NO yields a plausible explanation of the formation of N_2O via the sequence of Eqs. (4)–(6), which can now be written with the V_o coordinated by two Mn^{3+} ions and NO_{ads} as a nitrosyl group.

The conclusions to which this work leads are summarized as follows:

(1) NO adsorbs on manganite perovskites in molecular and in dissociative forms.

(2) Oxygen vacancies adjacent to a transition ion of variable valence are necessary for dissociative adsorption of NO.

(3) The concentration of oxygen vacancies is enhanced by the presence of charge-compensating defects such as cation vacancies, alkali ions, and alkaline earth ions substituted for La^{3+} ions. Cation vacancies are most effective.

(4) At constant Mn^{4+} content, lattice oxygen is less strongly bound for (La, □) MnO_3 than for (La, K) MnO_3 and this increases the activity of the former compound in comparison with the latter.

(5) The geometrical distortions of the basic perovskite cube are unimportant for the catalytic activity in NO reduction.

Acknowledgments

We thankfully acknowledge the electrical conductivity measurements made by J. V. Waszczak, the help in the desorbed gas analysis by Mrs. E. Vogel, and the surface area determinations by F. Schrey.

References

1. G. H. Jonker and J. H. van Santen, *Physica* **16**, 337 (1950).
2. J. H. van Santen and G. H. Jonker, *Physica* **16**, 599 (1950).

3. J. B. GOODENOUGH AND J. M. LONGO, "Landolt-Börnstein, New Series, Group III," Vol. 4a, p. 126, Springer-Verlag, Berlin (1970).
4. B. J. EVANS AND D. R. PEACOR, *J. Solid State Chem.* **7**, 36 (1973) and references therein.
5. F. K. LOTGERING, *Philips Res. Repts.* **25**, 8 (1970).
6. J. B. A. A. ELEMANS, B. VAN LAAR, K. R. VAN DER VEEN, AND B. O. LOOPSTRA, *J. Solid State Chem.* **3**, 238 (1971).
7. G. MATSUMOTO, *J. Phys. Soc. Japan* **29**, 606, 615 (1970).
8. B. C. TOFIELD AND W. R. SCOTT, *J. Solid State Chem.* **10**, 183 (1974).
9. G. PARRAVANO, *J. Am. Chem. Soc.* **75**, 1497 (1953).
10. R. J. H. VOORHOEVE, J. P. REMEIKA, P. E. FREELAND, AND B. T. MATTHIAS, *Science* **177**, 353 (1972).
11. R. J. H. VOORHOEVE, J. P. REMEIKA, AND D. W. JOHNSON, JR., *Science* **180**, 62 (1972).
12. E. G. VRIELAND, *J. Catal.* **32**, 415 (1974).
13. S. BRAUNAUER, P. H. EMMETT, AND E. TELLER, *J. Am. Chem. Soc.* **60**, 309 (1938).
14. R. J. H. VOORHOEVE, L. E. TRIMBLE, AND C. P. KHATTAK, *Mater. Res. Bull.* **9**, 655 (1974).
15. R. J. H. VOORHOEVE AND L. E. TRIMBLE, to be published.
16. H. L. YAKEL, JR., *Acta Cryst.* **8**, 394 (1955).
17. A. WOLD, R. J. ARNOTT, AND J. B. GOODENOUGH, *J. Appl. Phys.* **29**, 387 (1958).
18. W. C. KOEHLER AND E. O. WOLLAN, *J. Phys. Chem. Solids* **2**, 100 (1957).
19. E. O. WOLLAN AND W. C. KOEHLER, *Phys. Rev.* **100**, 545 (1955).
20. A. WOLD AND R. J. ARNOTT, *J. Phys. Chem. Solids* **9**, 176 (1959).
21. G. H. JONKER AND J. H. VAN SANTEN, *Physica* **19**, 120 (1953).
22. J. SCHRÖDER, *Z. Naturf.* **17B**, 346 (1962).
23. G. H. JONKER, *J. Appl. Phys.* **37**, 1424 (1966).
24. I. MATSUURA AND G. C. A. SCHUIT, *J. Catal.* **25**, 314 (1972) and references therein.
25. W. M. H. SACHTLER, *Catal. Rev.* **4**, 27 (1971).
26. E. R. S. WINTER, *J. Catal.* **22**, 158 (1971).
27. A. AMIRNAZMI, J. E. BENSON, AND M. BOUDART, *J. Catal.* **30**, 55 (1973).
28. R. J. H. VOORHOEVE, J. P. REMEIKA, AND L. E. TRIMBLE, *Mater. Res. Bull.* **9**, 1393 (1974).
29. T. WOLFRAM, E. A. KRAUT, AND F. J. MORIN, *Phys. Rev.* **B7**, 1677 (1973).
30. L. I. AHMAD, *Surface Sci.* **12**, 437 (1968).
31. R. J. H. VOORHOEVE AND J. P. REMEIKA, *in* "The Catalytic Chemistry of Nitrogen Oxides," General Motors Symposium, Warren, Mich, October 6–8, 1974, Plenum.
32. M. SHELEF AND J. T. KUMMER, *Chem. Eng. Progr.* **67**, 74 (1971).
33. H. C. YAO AND M. SHELEF, *J. Catal.* **31**, 377 (1973).